RSC Advances

PAPER

View Article Online
View Journal | View Issue



Cite this: *RSC Adv.*, 2021, **11**, 25801

# Theoretical study of ternary silver fluorides $AgMF_4$ (M = Cu, Ni, Co) formation at pressures up to 20 GPa†‡

Mateusz A. Domański,*[a] Mariana Derzsi [ab] and Wojciech Grochala *[a]

Received 27th June 2021
Accepted 15th July 2021

DOI: 10.1039/d1ra04970d

rsc.li/rsc-advances

Only several compounds bearing the Ag(II) cation and other paramagnetic transition metal cations are known experimentally. Herein, we predict *in silico* stability and crystal structures of hypothetical ternary silver(II) fluorides with copper, nickel and cobalt in 1 : 1 stoichiometry at a pressure range from 0 GPa up to 20 GPa employing the evolutionary algorithm in combination with DFT calculations. The calculations show that $AgCoF_4$ could be synthesized already at ambient conditions but this compound would host diamagnetic Ag(I) and high-spin Co(III). Although none of the compounds bearing Ag(II) could be preferred over binary substrates at ambient conditions, at increased pressure ternary fluorides of Ag(II) featuring Cu(II) and Ni(II) could be synthesized, in the pressure windows of 7–14 and 8–15 GPa, respectively. All title compounds would be semiconducting and demonstrate magnetic ordering. Compounds featuring Ni(II) and particularly Co(II) should exhibit fundamental band gaps much reduced with respect to pristine $AgF_2$. The presence of Cu(II) and Ni(II) does not lead to electronic doping to $AgF_2$ layers, while Co(II) tends to reduce Ag(II) entirely to Ag(I).

## Introduction

Recent experimental and theoretical research on $AgF_2$ demonstrated that this material mimics very closely the key structural and electronic properties of the well-known lanthanum oxocuprate $La_2CuO_4$ (ref. 1) – the prototype precursor of high-temperature oxocuprate superconductors – that are believed to be a necessary prerequisite for the unique behaviour of the latter. They account for strong antiferromagnetic coupling *via* a superexchange mechanism in two-dimensional sheets[2] and substantial mixing of ligand and metal states in the top of the valence band. Superconductivity is reached in the oxocuprates *via* chemical doping and because of the striking similarities, not observed in any other known compound, it was suggested that superconductivity could be obtained also in the related silver(II) fluorides if proper chemical doping to $AgF_2$ that would lead to metallization could be realized.[1,3,4] It is therefore highly desirable to examine various possibilities to modify its electronic and magnetic properties *via* doping.

Doping in essence is equivalent to the insertion of surplus holes or electrons into the chemical system. However, in contrast to cuprates, the bulk $AgF_2$ has so far resisted all doping attempts. The hole doping of $AgF_2$ could be introduced by F adatoms, but theoretical studies show that doping to this 001-type system *via* the addition of F atoms does not lead to a stable metallic phase.[5] Partial oxidation of Ag(II) is also difficult, due to the immensely strong oxidative character of Ag(III); compounds of Ag(III) are even more difficult to synthesize and manipulate than Ag(II) compounds.

Therefore, our attention turned to electron doping, which could be introduced in two general ways. The first one is provided by vacancies at anionic sites ($AgF_2 \rightarrow AgF_{2-\delta}$). Similarly, as with additional $F^-$, the study shows that the vacancies lead to clustering and phase separation without the prospect of obtaining a metallic phase.[5] The second possibility, that we focus on here, is to modify $AgF_2$ *via* substitution at the cationic site injecting the surplus electron. Early attempts to dope ternary silver fluorides (*e.g.* $KAgF_3$) in a manner analogous to cuprates, *i.e.* substituting partially M(I) cations with M(II), failed. Recent theoretical investigations suggest that electron doping to $AgF_2$ would not lead to a stable metallic phase due to a lattice polaronic effect and charge localization.[6] Therefore the remaining way to achieve electron doping in $AgF_2$ is to try partial isostructural substitution of Ag(II). By this, we mean to replace square planar Ag(II) in $AgF_2$ with another redox-active metal cation, M(II), so that the layered structure is preserved but the electrons may partly flow from M(II) to Ag(II). This type of doping has not been yet achieved experimentally. Thus, in this

[a]*Centre of New Technologies, University of Warsaw, S. Banacha 2C, 02-097 Warsaw, Poland. E-mail: m.domanski@cent.uw.edu.pl; w.grochala@cent.uw.edu.pl*

[b]*Advanced Technologies Research Institute, Faculty of Materials Science and Technology in Trnava, Slovak University of Technology in Bratislava, Trnava, 917 24, Slovakia*

† This work is dedicated to Prof. Gary Schrobilgen at his 75th birthday.

‡ Electronic supplementary information (ESI) available: Study of difluorides compression, detailed results of EA runs, electronic structure details at HP, crystal structures and vibration frequencies. See DOI: 10.1039/d1ra04970d

study, we explored new ternary phases bearing Ag(II), especially isostructural to $AgF_2$, to learn to what extent could the electronic structure of $AgF_2$ sheets be altered by the presence of other metal cations.

The natural choice for the M element is a transition metal which also presents octahedral coordination featuring Jahn–Teller distortion like Ag(II). Accordingly, we considered diverse ternary fluoride stoichiometries which may host strongly coupled $AgF_2$ sheets. Among ternary fluorides $Ag^{II}M_xF_y$, many transition metal systems have been successfully prepared so far,[3] *i.e.* for M = Au(III), Au(V), Nb(V), Ta(V), Ti(IV), Zr(IV), Hf(IV), Ru(V), Rh(IV), Ir(V), Pd(IV), Pt(IV), Pt(V), Mn(IV) and Cr(IV) ($AgMn^{IV}F_6$ (ref. 7) and $AgCr^{IV}F_6$ (ref. 8) structures not known). None of these fluorides host $[AgF_2]$ sheets or chains required for achieving strong antiferromagnetic coupling. Yet the great majority of these compounds contain closed-shell or low-spin cations which would not hold any magnetic interactions.

Late 3d-block transition metals, especially Cu, Ni and Co, seem to be promising candidates for electron doping due to their relative resistance towards oxidation in the fluoride environment while having partly filled d subshell. The redox potentials for the $M^{3+/}M^{2+}$ redox pairs decrease in the Cu > Ni > Co sequence. Experimentally, $CoF_3$ and $NiF_3$ (actually $Ni^{II}Ni^{IV}F_4$ (ref. 9)) are moderately stable in an inert atmosphere, and they constitute strong fluorinating agents. On the other hand, $CuF_3$ is quite unstable thermally and thermodynamically[10] (even more than $AgF_3$ (ref. 11)), thus minimizing the possibility of the intrinsic redox reaction between Ag(II) and Cu(II). Remarkably, such appealing synthesis has not been achieved experimentally yet, so no fluorides having Ag(II) and M(II) (M = Cu, Ni, Co) in any ratio are known, despite many similarities between these cations. There are, however, some examples of compounds with Ag(I) and M(III) valences. Among fluoride systems, only the Ag(I) Co(III) fluoride with $Ag_3CoF_6$ formula has been already described,[12] suggesting that as yet unobserved Ag(II)Co(II) pair might be just beyond the border of intrinsic redox reaction. Silver fluorides with M = Cu or Ni are not known, thus the forms bearing Ag(II) and M(II) or Ag(I) and M(III) can not be excluded. Furthermore, there are known ternary oxide systems having Ag(I) and M(III) with $AgMO_2$ formula (M = Cu, Ni, Co).[13–17] Oxide and fluoride systems of silver tend to differ dramatically, thus the question about the nature of the late 3d ternary fluorides remains open.

The theoretical search for ternary systems bearing initially divalent cations has the aim of verification if it could possibly form a metallic phase with Ag(II). Since ternary oxides with Ag : M ratio of 1 : 1 are known, here we decided to study ternary fluorides with the same ratio. To understand whether ternary fluorides bearing Ag(II) in combination with another transition metal (TM) constitute a viable synthetic target, we have examined here $AgMF_4$ systems with Cu, Ni and Co using Density Functional Theory (DFT) methods in combination with evolutionary algorithms for crystal structures' prediction.

Preliminary results showed that such systems are very close in terms of energy to the sum of binary substrates but have lower volume, suggesting they could be obtained at elevated pressures. It is well-known that pressure may affect to a great extent both the crystal structures and stability of chemical compounds.[19] High-pressure synthesis proved to be crucial in the synthesis of some transition metal compounds, *e.g.* copper oxyfluorides[18] (and references therein), as well as for inducing metallization,[19,20] the latter being not possible in pure $AgF_2$.[21] Thus, aside from variations of the chemical composition, we also study the impact of external pressure on crystal and electronic structure, and stability of $AgMF_4$ systems with respect to the mixture of binary fluorides, $AgF_2$ and $MF_2$ (M = Cu, Ni, Co). Since both stability and electronic properties may depend on pressure, we have investigated the effect of external pressure on the formation and properties of the title $AgMF_4$ compounds.

## Computational methods

This theoretical study is based on periodic electronic-structure calculations for solids carried out with Vienna *Ab initio* Simulation Package 5.4.4 (VASP) software using projector-augmented wave method.[22–24] We used the potentials set recommended by VASP with a 520 eV plane-wave energy cut-off. Energy calculations utilized collinearly spin-polarized DFT method using generalized gradient approximation functional PBEsol (*i.e.* solid-revised Perdew, Burke and Ernzerhof correlation–exchange functional[25]). The on-site electronic correlation was included with Hubbard and exchange repulsion terms ($U$ and $J$) using Dudarev's approach.[26,27] Geometry optimizations were done with $k$-spacing of $2\pi \times 0.024$ Å$^{-1}$ (using the Monkhorst–Pack scheme) and conjugate-gradient algorithm for ionic relaxation with the criteria of $10^{-7}$ eV for electronic self-consistent-field convergence and $10^{-5}$ eV for ionic cycles convergence. In this approach effective $U_{\mathrm{eff}} = U - J$, is considered, thus we used $U_{\mathrm{eff}}$ equal 4 eV (for Ag, Ni), 5 eV (Co) and 8 (Cu). These values were earlier used and validated in respective systems exhibiting +II oxidation state.[2,28–30]

In our quest for the lowest-energy crystal structure of hypothetical compounds of $AgCuF_4$, $AgNiF_4$ and $AgCoF_4$, we have initially tested various substitutions within the known crystal structure of $AgF_2$. We have tested also various prototypical $M^IM^{III}F_4$ structures, which allow for electron transfer between metal sites; notably, we presumed that electron-hungry Ag(II) could undergo reduction, with the concomitant $1 - e^-$ oxidation of its neighbouring TM cations. The three scrutinized 3d elements, Cu, Ni and Co, differ in terms of redox properties, electron count, $U$-induced splitting of upper and lower Hubbard d-bands, and degree of tetragonal distortion of $MF_6$ octahedra. All above-mentioned cations also have significantly smaller cationic radii than Ag(II). $AgMF_4$ (M = Cu, Ni, Co) fluorides were modelled in the appropriate $ABC_4$ structure types selected from the Inorganic Crystal Structure Database (ICSD). Furthermore, in each case, we have searched for the global minimum structure using evolutionary algorithms (EA) as implemented in the XtalOpt software[33] for crystal structure prediction. The starting pool (*i.e.* 1$^{st}$ generation) for each XtalOpt run constituted 30 initial random structures containing 2 or 4 formula units in the unit cell. After the pool of structures is optimized by VASP, XtalOpt selects the best possible candidates for the next generation, employs such operators as strain, exchange, ripple,

and crossover on the selected candidates, which form the next generation of structures. Such structure generation and optimization continue until the energy convergence is reached. The XtalOpt runs were performed for the three title stoichiometries of $AgMF_4$, at 0 and 10 GPa considering unit cells containing 2 to 4 formula units. XtalOpt runs were done in combination with DFT calculations using VASP optimizer. A four-step optimization procedure of each structure was performed increasing accuracy at each step, using DFT for the first two and DFT+U (*i.e.* with Dudarev's approach) approach for the last two steps. These calculations were performed with reduced convergence criteria ($5 \times 10^{-7}$ eV and $5 \times 10^{-5}$ eV for the electronic and ionic cycle, respectively) and *k*-point mesh ($2\pi \times 0.048$ Å$^{-1}$). For each system, we have obtained about optimized 500 structures (more in ESI, see Fig. S1 and S2‡). The selected lowest-energy EA structures were reoptimized with higher precision as described above. The XtalOpt is a robust tool that has been utilized more than sixty times in solid-state chemistry or physics applications.[34]

For selected systems, geometry optimization was additionally performed using the HSE06 hybrid functional[35] with a coarser *k*-spacing ($2\pi \times 0.048$ Å$^{-1}$). For the chosen systems we calculated the electronic density of states (DOS) with tetrahedron method and Blöchl corrections, with both DFT+U and HSE06.

Dynamic stability was investigated in VASP by calculating $\Gamma$-point vibrational frequencies, using the density functional perturbation theory method and the DFT+U framework.

For visualization of crystal structures, VESTA[36] software was used. Band structure plots were made using PyProcar library[37] and AFLOW[38] program.

## Results and discussion

The idea of pressure study originates from preliminary results, as numerous low-volume polymorphs have already been identified in the XtalOpt quest at ambient pressure (Fig. S1a, c and e‡). Consequently, we have studied the $AgMF_4$ phases in a range of hydrostatic pressure with the prospect of obtaining pressure-induced stability of $AgMF_4$ (M = Cu, Ni and Co) in respect to binary substrates $AgF_2$ and $MF_2$, and to evaluate the possibility of high-pressure metallization of the ternary silver(II) fluorides. The formation enthalpy of the lowest-energy polymorphs from the substrates was investigated in the 0–20 GPa pressure range. The pressure evolution for $AgMF_4$ systems with respect to the sum of those for the binary substrates in their most stable polymorphs is presented in Fig. 1. With our choice of $U_{eff}$ we successfully confirmed the experimentally observed pressure-induced phase transitions of $AgF_2$,[21] $CuF_2$,[31] $NiF_2$ (ref. 32) and $CoF_2$ (ref. 28 and 32) up to 20 GPa (note in ESI, see also Table S1 and Fig. S3,‡ these phase transitions are marked in Fig. 1). The phase-transition sequences in the considered stoichiometries were calculated with the described DFT+U framework assuming hydrostatic conditions.

Additional insight into pressure-induced effects on the enthalpy of formation of the ternary fluorides comes from pV term analysis (ESI, Fig. S4‡). Both for low pressure (<3 GPa) and high-pressure range (>9 GPa) the pV factor works against the formation of the studied ternary fluoride phases. Consequently, the ternary fluoride phases benefit from the pV term with respect to the substrates in the range 3–9 GPa; at higher pressures, binary substrates experience volume-reducing phase transitions which reduces this advantage. The crucial is the phase transition of constituent $AgF_2$ at about 14 GPa into an unprecedented inorganic nanotube.[21] This incredibly low-volume polymorph reduces the pV term of substrates and gradually destabilizes thermodynamically all proposed ternary fluorides at pressures approaching 20 GPa. These factors result in re-entrant instability of the ternary phases above certain characteristic pressure in each case.

The hypothetical mixed-cation $AgMF_4$ fluorides from Fig. 1 are below described in the order of M = Cu, Ni, Co, in terms of their structure and stability, and then of the pressure effects. Finally, we investigate their electronic properties at ambient and elevated pressures.

### Copper

**Ambient pressure.** Due to the similar chemistry of Ag(II) and Cu(II), as well as similar crystal structures of binary fluorides,

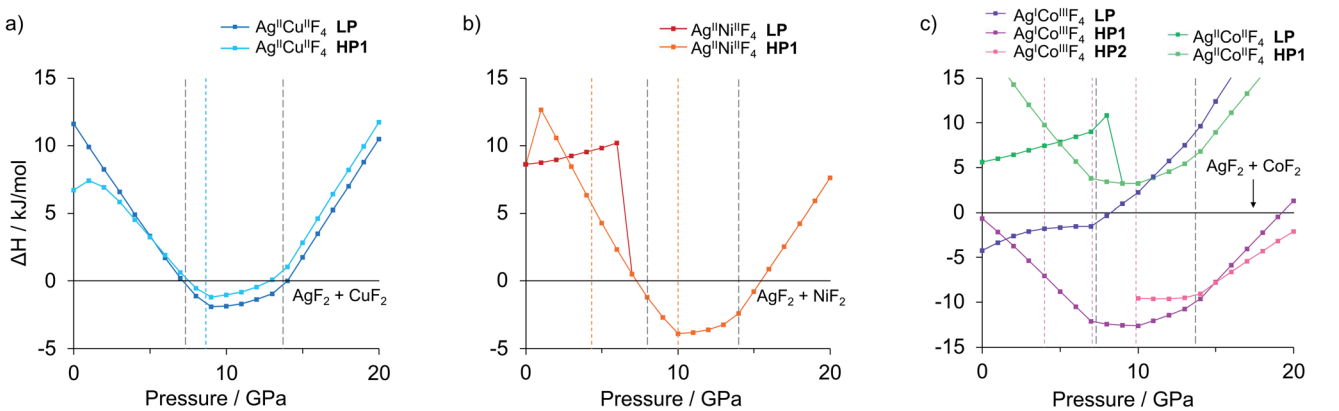


Fig. 1 Calculated relative enthalpy of ternary silver fluorides $AgMF_4$ (a) M = Cu, (b) M = Ni, (c) M = Co, with respect to lowest-enthalpy polymorphic forms of binary fluorides at each given pressure point. All the lowest enthalpy Ag(II)–M(II) fluorides comprise M-half-substituted $AgF_2$ type structures. Vertical dashed lines indicate phase transitions calculated for the $MF_2$ substrates.

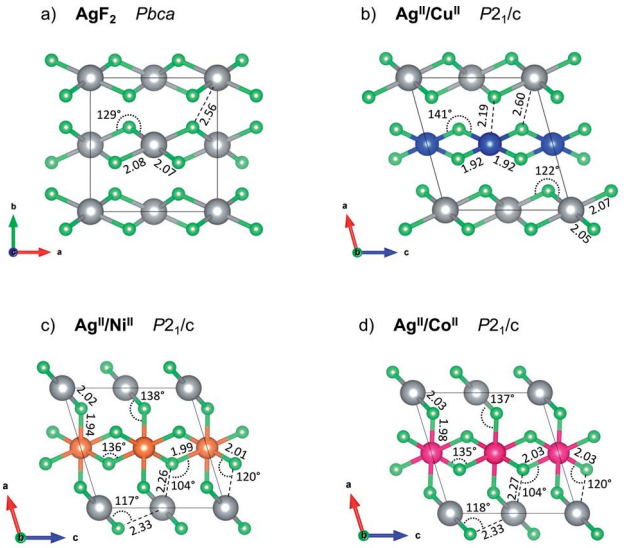


Fig. 2 Crystal structures of (a) parent $AgF_2$, the lowest-energy predicted (b) $AgCuF_4$, and (c) $AgNiF_4$, and metastable (d) $Ag^{II}Co^{II}F_4$ at ambient pressure (LP structure of each). The threshold for Ag–F bond drawing is 2.15 Å in all cases. All bond lengths provided in angstroms, and angles in degrees. Grey for silver atoms, green for fluorine, blue for copper, orange for nickel and magenta for cobalt.

our primary candidate for the $AgCuF_4$ structure was the orthorhombic layered structure typical of $AgF_2$ (ref. 39) (Fig. 2a). Three types of substitutions at the metal site were considered, *i.e.* metal alternation in the directions perpendicular to the $\vec{a}, \vec{b}$ or $\vec{c}$ lattice vectors (*cf.* ESI, Fig. S5‡). Notably, these three diverse polymorphs were also found during EA search (see ESI, Fig. S1 and S2‡). We found that a monoclinic variant of the $AgF_2$ type structure with metal alternation in the original *b* direction is the lowest-energy structure of $AgCuF_4$ (marked here as low-pressure, LP, structure, Fig. 2b), as confirmed by evolutionary algorithm quest. This polymorph preserves the layered character of its binary constituents by separating Ag and Cu into distinct puckered $[AgF_{4/2}]$ and $[CuF_{4/2}]$ layers. Substantial axial elongation of both Ag(II) and Cu(II) octahedra is predicted (*i.e.* four shorter equatorial and two considerably longer axial Ag(Cu)–F distances (2 + 2) + 2 coordination), in agreement with the strong Jahn–Teller effect which is expected for $d^9$ species in octahedral field. The rhombic distortion can be approximated to tetragonal distortion (4) + 2 in most cases. The ratio of axial to equatorial bond lengths $R = d_{ax}/d_{eq}$ (dimensionless Jahn–Teller distortion parameter often used to describe such compounds[40]) equals 1.24 for the Ag(II) site and 1.14 for the Cu(II) one. The tetragonal distortion for both cations is similar as in the parent phases where this ratio equals 1.23 and 1.15, for $AgF_2$ and $CuF_2$, respectively (all geometry parameters are summarised in Table 1).

Axial elongation suggests that in both cations d-hole occupies $d_{x^2-y^2}$ orbital. Both constituent layers $[AgF_{4/2}]$ and $[CuF_{4/2}]$ of $AgCuF_4$ preserve intra-sheet antiferromagnetic ordering.

The geometry within the puckered layers is reminiscent of those found in binary fluorides; the $[AgF_{4/2}]$ layers are more buckled than in pure $AgF_2$ (the Ag–F–Ag angle is 122° *vs.* 129° in bulk $AgF_2$), while $[CuF_{4/2}]$ layers are flattened (the corresponding angle is 141° *vs.* 132° in bulk $CuF_2$). This feature stems from the difference in the ionic radii between Ag(II) and Cu(II). In order to form a segregated layer structure, the $[AgF_2]$ sheets must buckle and the $[CuF_2]$ sheets must simultaneously flatten; this accommodation is associated by bending of the crystallographic beta angle from 90° (for bulk $AgF_2$) to 105°. We notice that two other models with mixed $[(Ag,Cu)F_{4/2}]$ layers (ESI, Fig. S5c and d‡), have energies higher by +6.4 and +7.3 kJ $mol^{-1}$, respectively, as compared to the LP structure. We also found a crystal structure containing Ag–F–Cu bridges and exhibiting genuine 3D connectivity (Fig. S5b‡), characterized by much lower volume. Importantly, the most stable LP polymorph is computed to be +6.7 kJ $mol^{-1}$ uphill in energy with respect to substrates:

$$AgF_2 + CuF_2 \rightarrow AgCuF_4 \quad (1)$$

Thus, if prepared, this ternary fluoride might be only metastable. However, its kinetic stability with respect to phase separation is indicated by our phonons calculations, yielding no imaginary frequencies for this polymorph (Appendix S4,‡ the same is true for all structures examined in this work).

**High pressures.** In the case of $AgCuF_4$ system, the LP layered $Ag^{II}Cu^{II}F_4$ structure is predicted to transform to a high-pressure $Ag^{II}Cu^{II}F_4$ polymorph (Fig. 3b, denoted HP1) with three-dimensional connectivity. The phase transition to the HP1

Table 1 Key geometry parameters of structures of parent $AgF_2$ and ternary silver fluorides $Ag^{II}M^{II}F_4$ (M = Cu, Ni, Cu) at ambient and increased pressure. Also, octahedral distortion parameter *R* is provided. N.D. stands for 'not determined' which is due to strong rhombic distortion

| | | | Bond length (Å) | | | | Bond length (Å) | | | |
|---|---|---|---|---|---|---|---|---|---|---|
| System | Label | *p* (GPa) | Ag–$F_1$ | Ag–$F_2$ | Ag–$F_3$ | *R* | M–$F_1$ | M–$F_2$ | M–$F_3$ | *R* |
| $Ag^{II}F_2$ | LP | 0 | 2.07 | 2.08 | 2.56 | 1.23 | — | — | — | — |
| | HP1 | 10 | 2.06 | 2.06 | 2.37 | 1.15 | — | — | — | — |
| $Ag^{II}Cu^{II}F_4$ | LP | 0 | 2.05 | 2.07 | 2.60 | 1.26 | 1.92 | 1.92 | 2.19 | 1.14 |
| | HP1 | 10 | 2.03 | 2.10 | 2.38 | 1.15 | 1.85 | 1.91 | 2.15 | 1.14 |
| $Ag^{II}Ni^{II}F_4$ | LP | 0 | 2.02 | 2.26 | 2.33 | 0.88 | 1.94 | 1.99 | 2.01 | 0.97 |
| | HP1 | 10 | 2.02 | 2.11 | 2.43 | 1.18 | 1.93 | 1.94 | 1.95 | 0.99 |
| $Ag^{II}CoF_4$ | LP | 0 | 2.03 | 2.27 | 2.33 | 0.88 | 1.98 | 2.03 | 2.03 | 0.98 |
| | HP1 | 10 | 2.01 | 2.18 | 2.33 | N.D. | 1.92 | 2.00 | 2.03 | 0.95 |

structure takes place around 6 GPa. The HP1 form remains energetically favoured over the LP one up to the highest calculated pressure of 20 GPa (Fig. 1a). Moreover, HP1 would become stable with respect to the substrates in the pressure range of about 7–14 GPa with the minimum relative enthalpy ($-1.9$ kJ mol$^{-1}$, in eqn (1)) reached *ca.* 9 GPa.

The HP1 polymorph is also based on the $AgF_2$ type structure, but the fluorine bridges are now formed between the two chemically distinct metal cations (Ag–F–Cu) in contrary to the LP structure, where fluorine atoms bridge metal cations of the same type (Ag–F–Ag and Cu–F–Cu). One can think of the HP1 structure as the LP one with direct Jahn–Teller elongation taking place within the $[AgF_{4/2}]$ and $[CuF_{4/2}]$ layers (alternating along $\vec{b}$ or $\vec{c}$) instead of in the direction perpendicular to the layers (along $\vec{a}$). Consequently, the 2D connectivity within the $[AgF_{4/2}]$ and $[CuF_{4/2}]$ layers is broken and a 3D Ag–F–Cu one established with the cooperative Jahn–Teller mechanism. The HP1 form of $AgCuF_4$ has a ferrimagnetic character with a small uncompensated spin (*ca.* 0.02 $\mu_B$) due to opposite spin on Ag(II) and Cu(II) cations with slightly different magnetic moments on each type of TM cation. Like in the LP polymorph, here the Cu and Ag octahedra are both axially elongated, see Table 1.

## Nickel

**Ambient pressure.** Predictions of the crystal structure of $AgNiF_4$ – in contrast to those featuring Cu(II) – were influenced by the fact that Ni(II) reveals a known tendency to be oxidized to Ni(III) or even Ni(IV), though higher fluorides of nickel tend to release $F_2$.[41] However, during our quest only very few such structures with intervalence charge transfer were found, having considerably higher enthalpy (*i.e.* at least +56.4 kJ mol$^{-1}$, Fig. S1c‡). Similarly, as in the case of Cu(II), the lowest-energy structure of $AgNiF_4$ is a monoclinic variant of the parent $AgF_2$ type structure, with a slightly larger beta angle of 107° compared to the LP $AgCuF_4$. However, in contrast to $AgF_2$ and LP $AgCuF_4$, the nickel compound is not layered. The Ag(II) cations are subject to inverse Jahn–Teller effect with axial compression of the $AgF_6$ octahedra taking place in the direction perpendicular to the $[AgF_{4/2}]$ layers and with the *R* ratio equal to 0.88 (Fig. 2c and Table 1). The axial compression manifested by presence of quasi-dumbbell Ag(II) is known from the fluorine chemistry of Ag(II)[42] and leads to d-hole sitting in $d_{z^2}$ orbital. On the other hand, the $NiF_6$ octahedra remain nearly undistorted with *R* ratio equal to 0.97 (compared to 0.98 calculated for rutile $NiF_2$), as typical for high-spin Ni(II). Consequently the Ag(II) cations act as connectors between octahedral $[NiF_{4/2}F_{2/1}]^{2-}$ layers present within the *bc* plane. The axial Ag–F bonds involved in the formation of the Ag–F–Ni bridges are shorter than the equatorial Ag–F bonds within the $[AgF_{2/4}]$ layers (Table 1). The cooperative Jahn–Teller effect results in LP $AgNiF_4$ structure with a three-dimensional Ag(II)Ni(II)$F_4$ network and antiferromagnetic coupling between Ag(II) and Ni(II) sites. This LP structure is the lowest energy among all structures found at 0 GPa, but it still has energy +8.6 kJ mol$^{-1}$ with respect to the binary substrates $AgF_2$ + $NiF_2$. However, it exhibits no imaginary phonon modes (Appendix S4‡) which points to its kinetic stability. Therefore, if synthesized, $AgNiF_4$ should be metastable at ambient pressure, similarly to $AgCuF_4$.

**High pressures.** In the $AgNiF_4$ system, similar high-pressure behaviour is predicted for $AgCuF_4$, and despite a different electron count on TM. Namely, the high pressures preserve the Ag(II) oxidation state and promote the increase of lattice connectivity by the cooperative Jahn–Teller mechanism. Under elevated pressures, the LP → HP1 transition is predicted to take place at 3 GPa (Fig. 1b). The axial compression in LP of Ag(II) is electronically stable only up to 6 GPa. Above this pressure, it vanishes, which is manifested in Fig. 1b by merging the LP curve with the HP1 from 7 GPa. The HP1 has negative enthalpy as compared to the binary fluorides from the pressure of 7 GPa up to ~15 GPa (Fig. 1b). The maximum stabilization of $AgNiF_4$ relative to binary substrates reaches $-3.9$ kJ mol$^{-1}$ at 10 GPa. $AgNiF_4$ HP1 form remains the only high-pressure $AgNiF_4$ structure predicted by us up to 20 GPa. Due to small structural differences between both proposed $AgNiF_4$ structures, it may be expected that if HP1 structure was synthesized under high pressure it would decompress to its LP form without large internal strain.[43]

In contrast to $AgCuF_4$, however, the HP1 $Ag^{II}Ni^{II}F_4$ structure emerges from the LP one while changing axial compression of Ag(II) cations to an elongation, taking place perpendicular to the $[AgF_{4/2}]$ layers and resulting in a hole in $d_{x^2-y^2}$ orbital. Consequently, two-dimensional connectivity within the $[AgF_{4/2}]$ is established (Fig. 3c) in contrary to the situation in the LP form, where the Jahn–Teller distortion is responsible for no connectivity with the silver layers (Fig. 2c). Thus, the LP and HP1 $Ag^{II}Ni^{II}F_4$ structures differ topologically mainly by 2D Ag–F–Ag connectivity in the latter compared to no such connectivity in the former. The HP1 polymorph may be thought of as build

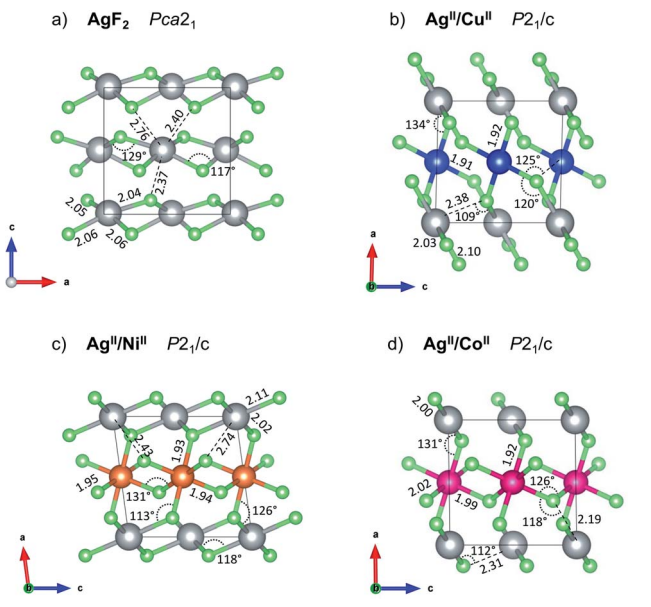


Fig. 3 Crystal structures of (a) parent $AgF_2$, and the lowest-energy predicted (b) $AgCuF_4$, and (c) $AgNiF_4$, and metastable (d) $Ag^{II}Co^{II}F_4$ at 10 GPa (HP1 structure of each). The threshold for Ag–F bond drawing is 2.15 Å in all cases. Another view of these structures is shown in ESI, Fig. S6.‡

from separate antiferromagnetic layers of $[AgF_{4/2}]$ and $[NiF_{4/2}]$ parallel to *bc* plane.

### Cobalt

**Ambient pressure.** Interestingly, in the case of $AgCoF_4$, the difference between standard reduction potentials for the $Co^{3+/2+}$ and $Ag^{2+/1+}$ redox pairs is considerable (1.82 V *vs.* 1.98 V,[44] respectively), so a reaction:

$$AgF_2 + CoF_2 \rightarrow AgF + CoF_3 \quad (2)$$

could be expected. Calculations show that this reaction between binary fluorides would not be favoured though, on both DFT+U level of theory (+25.8 kJ mol$^{-1}$) or hybrid density functional HSE06 (+12.2 kJ mol$^{-1}$, see HSE06 results for all the binary and ternary compounds in ESI, Table S2‡). Having learned that, we tried to stabilize the $Ag^{II}Co^{II}F_4$ solution. This $Ag^{II}Co^{II}F_4$ LP polymorph (Fig. 2d) is isostructural with the lowest-energy $Ag^{II}Ni^{II}F_4$ LP structure. It exhibits the same inverse Jahn–Teller distortion pattern as the one described above in $Ag^{II}Ni^{II}F_4$ structure, *i.e.* substantial axial compression of Ag(II) sites and much smaller distortion at Co(II) sites, indicating that their half-filled orbitals are directed towards each other. This, together with a sufficiently large Ag–F–Co angle results in an antiferromagnetic ground state which, however, is at +5.7 kJ mol$^{-1}$ above binary divalent substrates.

Importantly, it appears that the lowest-energy mixed-cation structure obtained in the cobalt system corresponds to the $Ag^{I}Co^{III}F_4$ formulation, for which we also found the lowest-energy $Ag^{I}Co^{III}F_4$ polymorph. Structure quests using evolutionary algorithms resulted in many similar layered $Ag^{I}Co^{III}F_4$ structures, including $KFeF_4$-HT polymorph ($Z = 4$, for others, see ESI, Fig. S1 and S2‡). Further modifications helped us finding the lowest-energy $Ag^{I}Co^{III}F_4$ LP polymorph in the $KFeF_4$-LT[45] type structure ($Z = 8$, Fig. 4a). DFT+U calculations yield the energy of this structure to be −4.2 kJ mol$^{-1}$ (or −24.8 kJ mol$^{-1}$ at HSE06 level) with respect to the binary divalent metal fluorides. It also turns out that the energy for the Lewis acid–Lewis base reaction:

$$AgF + CoF_3 \rightarrow Ag^{I}Co^{III}F_4 \quad (3)$$

is negative, about −34.8 kJ mol$^{-1}$ at DFT+U level (−37.4 kJ mol$^{-1}$ at HSE06 level, Table S2‡), and it compensates for the unfavourable energy of the redox reaction (eqn (2)). Even for the models derived from parent $AgF_2$ type structure suitable to host Ag(II), the spontaneous electron-transfer reaction takes place; it manifests itself by the disappearance of the spin on Ag site and change of magnetic moment on the Co site. The reaction described by eqn (3) has a close analogue for other stoichiometry; the known cryolite type $Ag_3CoF_6$ contains no Ag(II), and its formula may be written as $Ag^{I}{}_3Co^{III}F_6$.

The $KFeF_4$-LT type structure comprises the puckered antiferromagnetic anionic sheets of $[CoF_{4/2}F_{2/1}]^-$ stoichiometry which features high-spin Co(III) cations, and diamagnetic Ag(I) counterions. While in parent $CoF_3$ the octahedra are almost perfectly symmetric (with all bond lengths of 1.89 Å, the F–Co–F angles are distorted ±1.5° from 90°), in $Ag^{I}Co^{III}F_4$ the $CoF_6$ octahedra are markedly compressed with axial bond length 1.82 Å resulting in *R* ratio equal 0.94 (equatorial bonds are highlighted on Fig. 4a). Considering the coordination sphere of Ag(I), pristine AgF crystalizes in rock-salt structure with regular octahedra having 2.426 Å Ag–F bond lengths. In the case of $AgCoF_4$, however, two types of Ag(I) can be distinguished, each with coordination number, CN = 7 within 2.65 Å radius, and both in the form of a bicapped tetragonal pyramid.

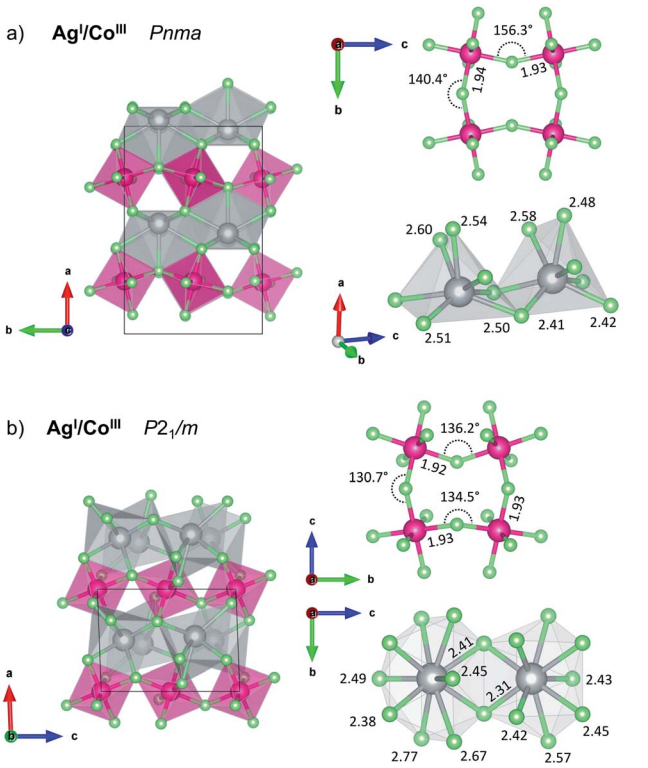


Fig. 4 Structure of $Ag^{I}Co^{III}F_4$ at (a) ambient and (b) elevated pressure (10 GPa), with selected geometric parameters of Ag(I) coordination polyhedra and $[CoF_{4/2}F_{2/1}]$ sheets. The threshold for Ag–F bond drawing is 2.7 Å in $Ag^{I}Co^{III}F_4$ structures.

**High pressures.** Comparing to Ni and Cu systems, richer polymorphism is predicted under elevated pressures in the $AgCoF_4$ system. The $Ag^{II}Co^{II}F_4$ solution gains stability at elevated pressures, forming the HP1 polymorph, which resembles the HP1 polymorph of $AgCuF_4$ described above (Fig. 3d). Ag(II) sites in $Ag^{II}Co^{II}F_4$ HP1 are far more axially compressed, suggesting a d-hole occupation mainly of $d_{z^2}$ orbital oriented towards Co(II) sites. The Ag–F–Co bridges with 131° angle form chains leading to an antiferromagnetic ground state. The HP1 is favoured over LP polymorph above 5 GPa, but it would not be stabilized under high pressure like Ni and Cu systems. The relative enthalpy of $Ag^{II}Co^{II}F_4$ HP1 with respect to the parent divalent fluorides reaches a local minimum at about 9–10 GPa with +3.2 kJ mol$^{-1}$ (Fig. 1c, green series).

Likewise, at ambient pressure conditions, the intrinsic redox reaction in $AgCoF_4$ system is favoured at elevated pressures. Here the lowest-energy mixed valence LP $Ag^{I}Co^{III}F_4$ is predicted to undergo two subsequent high-pressure transitions at about

1 GPa (HP1) and 15 GPa (HP2), respectively while maintaining the metal oxidation states (Fig. 1c, magenta series). Both, HP1 and HP2 forms represent $KMnF_4$ type structures similarly as the LP one but with reduced symmetry according to the sequence *Pmna* (LP) → $P2_1/m$ (HP1) → $C2/c$ (HP2). Apparently, it turns out that $Ag^{I}Co^{III}F_4$ stability would increase under high pressure about threefold with respect to substrates at 10 GPa, up to −12.6 kJ $mol^{-1}$.

The first $Ag^{I}Co^{III}F_4$ high-pressure polymorph HP1 was found at 10 GPa using EA has a distorted monoclinic $KMnF_4$ type structure (Fig. 4b). This polymorph of $Ag^{I}Co^{III}F_4$ resembles the LP polymorph having antiferromagnetic puckered sheets of $[CoF_{4/2}F_{2/1}]^-$ stoichiometry with high-spin Co(III) cations and diamagnetic Ag(I) in between. Volume decrease of $Ag^{I}Co^{III}F_4$ with respect to binary fluorides is mainly due to enhancement of $[CoF_{4/2}F_{2/1}]^-$ layers buckling and increase of Ag(I) coordination number. Antiferromagnetic sheets are built from $CoF_6$ octahedra exhibiting axial bond compression with $R$ ratio equal 0.92 (axial bonds are 1.78 Å, equatorial 1.92–1.93 Å, *cf.* Fig. 4b). The equatorial Co–F bonds form a layer parallel to the *bc* plane. The Ag(I) cation is found at 10 GPa in two distinct crystallographic sites which differ in their coordination number. Here, CN is either 9 or 10, with bond lengths varying from 2.31 up to 2.77 Å. For comparison, at the same pressure, parent AgF is found in the CsCl type structure with cubic coordination sphere (8 ligands) and Ag–F bond length of 2.47 Å. The second high pressure polymorph of $Ag^{I}Co^{III}F_4$ $Ag^{I}Co^{III}F_4$ also crystallizes in $KMnF_4$ type structure ($C2/c$). It features higher CN for Ag(I) sites and more buckled $[CoF_{4/2}F_{2/1}]^-$ layers.

## Electronic properties

The main motivation behind studying novel ternary Ag(II) fluorides is to achieve appreciable changes in electronic structure that would result in facile metallization within the $[AgF_2]$ layers either at ambient or elevated pressures. To evaluate this possibility, we first discuss the electronic density of states (DOS) computed for $AgF_2$ and the studied ternary $AgMF_4$ fluorides at DFT+U level and zero pressure. Subsequently, we discuss the impact of pressure on their bandgaps.

**Ambient pressure.** The total and orbital-projected electronic DOS plots at ambient pressure are shown in Fig. 5. The DOS of the parent $AgF_2$ (Fig. 5a) shows a narrow band gap (1.33 eV) with a strong mixture of Ag 4d and F 2p orbitals around the Fermi level, with the Ag states dominate the lower-energy valence DOS and F states dominate the higher-energy valence DOS.[1,30] The gap opens between valence bands of predominantly F character and conduction bands of predominantly Ag character. The lowest-energy conduction band (centred around 1.5 eV) and the lowest-energy valence band (∼−6.5 eV) represent the upper and lower Hubbard band (UHB and LHB; marked with red arrows in Fig. 5) of dominant Ag $d_{x^2-y^2}$ character, respectively. The large separation of these bands on the energy scale and their position relative to F states define $AgF_2$ as a charge-transfer (CT) insulator according to the Zaanen–Sawatzky–Allen classification scheme.[46]

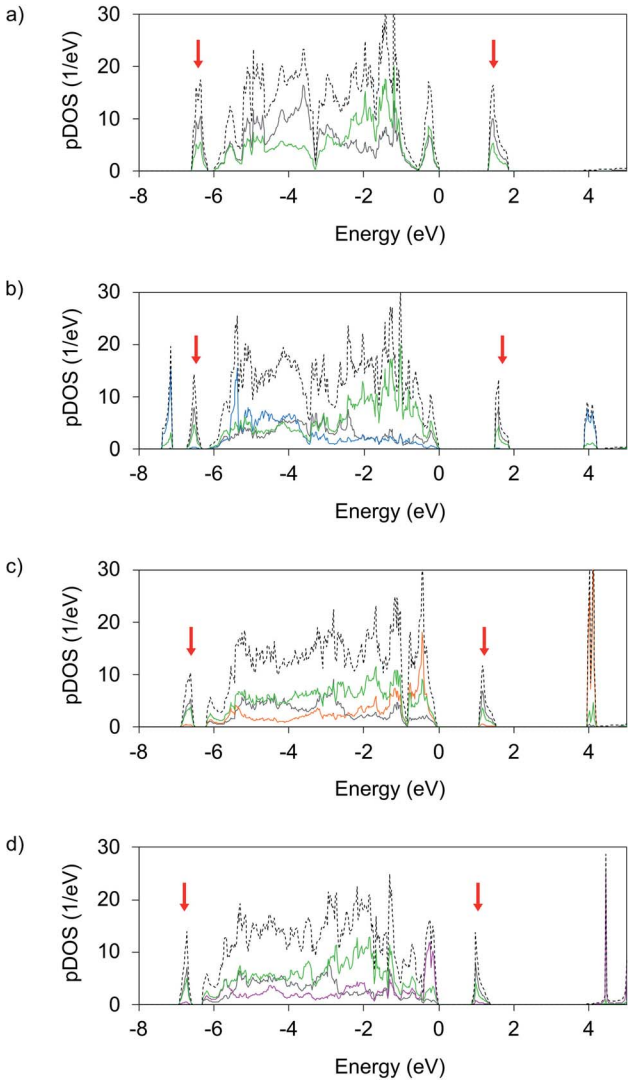


Fig. 5 Orbital projected electronic density of states (pDOS) calculated on DFT+U level for (a) parent $AgF_2$, (b) $Ag^{II}Cu^{II}F_4$, (c) $Ag^{II}Ni^{II}F_4$, and (d) $Ag^{II}Co^{II}F_4$ compounds at 0 GPa. Red arrows indicate lower and upper Hubbard (LHB and UHB) bands of $Ag^{2+}$. Dashed lines indicate total DOS, Ag states are drawn in grey, F in green, Cu in blue, Ni in orange and Co in magenta. Fermi level is set to zero. Spin-up and spin-down states were summed up.

Analysis of the LP $Ag^{II}Cu^{II}F_4$ electronic DOS (Fig. 5b) shows that the formation of this compound does not lead to significant electronic changes within the $[AgF_{4/2}]$ layers with respect to pristine $AgF_2$. The main difference is the presence of Cu 3d states. The Cu valence states show similar distribution as the valence Ag states, while the LHB (∼7.5 eV) and UHB (∼4 eV) of Cu display even larger separation than the Ag ones, which reflects the larger U at Cu(II) sites. Consequently, the nature of the bandgap of $AgCuF_4$ is defined by the bandgap of the $[AgF_{4/2}]$ sublayer. It is only slightly broader than in the parent $AgF_2$ (1.46 eV *vs.* 1.33 eV). Evidently, both the $[AgF_{4/2}]$ and $[CuF_{4/2}]$ layers in $AgCuF_4$ are well electronically separated, preserving the nature of their respective substrates, *i.e.* insulating character associated with a ligand to metal CT gap.

More significant changes *vs.* $AgF_2$ are observed in the DOS for $AgNiF_4$ (Fig. 5c). Here, the additional Ni 3d states predominate the valence DOS at the highest energies below the Fermi level and on average above the F 2p valence states. This contrasts $AgF_2$ and $AgCuF_4$ DOS, where the metal states are on average shifted to lower energies relative to F 2p valence states. Due to the appearance of the Ni states at higher energies the position of the Ni LHB is positioned just below the Fermi level, while the conduction band preserves the character of the Ag UHB band level. This means that the CT character of the bandgap has changed. Now the charge transfer is realized between the valence states of dominant Ni and conduction states of dominant Ag character. The appearance of Ni 3d states above the F 2p states of valence DOS results in a noticeably narrower band gap (1.09 eV) than in parent $AgF_2$ (1.33 e).

In the case of $Ag^{II}Co^{II}F_4$, the Co 3d (Fig. 5d) valence states are shifted to even higher energies relative to the F 2p valence resulting in an even narrower bandgap of 0.90 eV. The Co LHB positioned just below the Fermi level has almost the entire Co character, meaning that charge transfer over the bandgap is now from Co(II) states to the UHB of Ag(II), and indicate the proximity of intrinsic redox reaction character.

Noticeably, the band gaps of $Ag^{II}Ni^{II}F_4$ and $Ag^{II}Co^{II}F_4$ have an intervalence CT character, with Ni(II)/Co(II) serving as an electron donor, and Ag(II) as an acceptor, the intervalence CT being more pronounced in $Ag^{II}Co^{II}F_4$. The picture of $Ag^{I}Co^{III}F_4$ is reversed relative to both $Ag^{II}Co^{II}F_4$ and $Ag^{II}Ni^{II}F_4$, here the top of the valence band mainly consists of filled 4d states of Ag(I) while the bottom of the conduction band corresponds to the UHB of Co(III) (Fig. S7a‡). Due to the intrinsic redox reaction discussed above band gap increases up to 2.02 eV, it is thus larger than that of $AgF_2$, and of the $Ag^{II}M^{II}F_4$ analogues.

Clearly, the electronic structure of $AgMF_4$ compounds in the series M = Cu, Ni, Co, changes together with the redox properties of M(II) cations. The gradual change of M bands contribution to the valence band is apparent on band structure plots, Fig. S8,‡ as well as in DOS (Fig. 5). For $AgCuF_4$, with Cu(III) in fluoride environment is experimentally accessible with the greatest difficulty, $AgCuF_4$ preserves Ag(II) and Cu(II) oxidation states and a ligand to metal CT insulator character. For $AgNiF_4$, where Ni(III) forms easier, electronic DOS reveals moderate ease of intervalence CT between Ni(II) donor and Ag(II) acceptor, with the corresponding valence and conduction bands separated by a mere ~1.1 eV. Finally, for $Ag^{I}Co^{III}F_4$, where Co(III) is most accessible, a genuine redox reaction is seen which leads to "inverse" intervalence CT character, where Ag(I) serves as an electron donor, while Co(III) as an acceptor. Note that our hybrid DFT (HSE06) calculations yielded qualitatively similar results for the ambient pressure $AgMF_4$ structures (Fig. S9‡).

**Increased pressures.** Fig. 6 shows the evolution of the bandgap with pressure in all modelled $AgMF_4$ systems. The band gap of $Ag^{II}Cu^{II}F_4$ remains almost constant about 1.5 eV up to 20 GPa, while experiencing only a slight increase upon the LP → HP1 phase transition at ~6 GPa. Interestingly in $Ag^{II}Ni^{II}F_4$ the LP → HP1 transition at ~3 GPa is accompanied by severe reduction of the band gap by a factor of two from ~1.1 to ~0.6 eV. After the transition, however, the band gap remains almost unchanged up to 20 GPa, excluding the prospect of its metallization. These features suggest the intervalence CT character of $AgNiF_4$ and a certain propensity towards redox process yielding higher oxidation states of Ni, with a concomitant reduction of Ag(II) to Ag(I). On the other hand, band gap of $Ag^{II}Co^{II}F_4$ decreases monotonically throughout the entire pressure range, but its reduction is nevertheless small, and the band gap equals ~0.7 eV at 20 GPa, so the pressure does not provide an opportunity for its metallization below 20 GPa either. The picture of $Ag^{I}Co^{III}F_4$ is the opposite, its bandgap is increased with every phase transition after which it only slowly monotonically decreases. Consequently, the bandgap at 20 GPa is even slightly higher (2.1 eV) than the 0 GPa value of 2.0 eV.

## Conclusions

The silver(II) fluoride system is theoretically predicted to resist forming ternary fluorides with Cu, and Ni fluorides at ambient pressure conditions. The isostructural substitution is largely unfavoured at ambient pressure due to excessive differences in Ag(II) and M(II) bond lengths and in the extent of their tetragonal distortion. The energies of formation of $Ag^{II}Cu^{II}F_4$ and

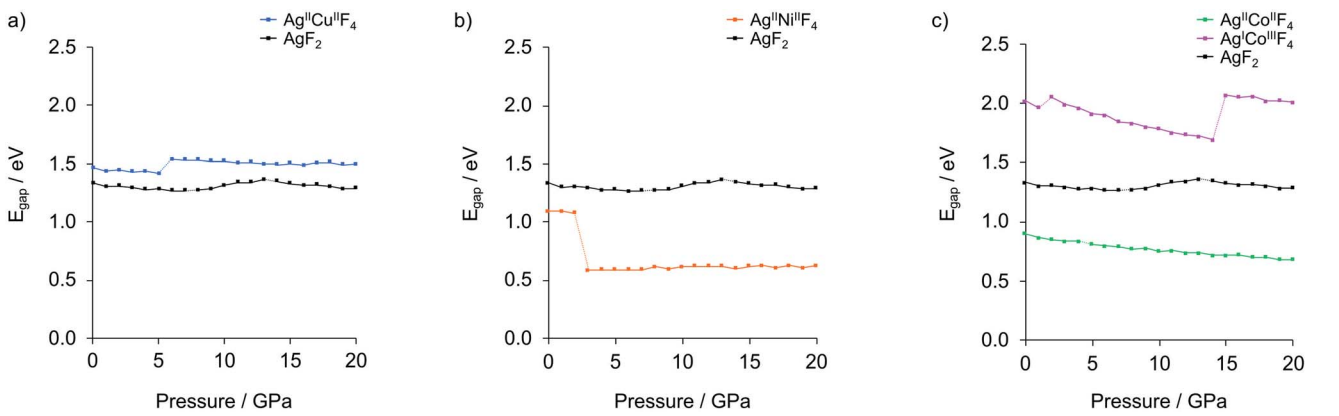


Fig. 6 Electronic band gaps dependency on pressure elevation for the lowest-enthalpy structures of (a) $AgCuF_4$, (b) $AgNiF_4$ and (c) $AgCoF_4$ (shown together with $AgF_2$). Dotted lines connect values calculated for structures separated by phase transitions. Detailed data is provided in Table S3.‡

$Ag^{II}Ni^{II}F_4$ are positive but these compounds have real phonon frequencies, hence could be metastable if prepared. Both $Ag^{II}Cu^{II}F_4$ and $Ag^{II}Ni^{II}F_4$ are predicted to be semiconductors with a predominant charge-transfer character. There is a clear trend in electronic band gaps and character of the states at the top of the valence band as one moves from Cu, *via* Ni to Co. The $AgCuF_4$ system has a comparable band gap with that of pristine $AgF_2$ at ambient pressure (1.46 eV *vs.* 1.33 eV), while $AgNiF_4$ system features a narrower band gap (1.09 eV).

The cobalt(II) system displays many similarities to both nickel and copper structures while having an even smaller band gap (0.90 eV). However, $Ag^{II}Co^{II}F_4$ configuration is predicted to be energetically unstable due to the potent oxidizing properties of Ag(II). The cobalt–silver fluoride system is thus quite different from the other two due to the intrinsic redox process resulting in a preference for as yet unknown $Ag^{I}Co^{III}F_4$. The ambient-pressure $KFeF_4$ type structure of this species is computed to be a *ca.* 2.02 eV band gap semiconductor, stable with respect to binaries and featuring antiferromagnetic sheets of $[CoF_{4/2}F_{2/1}]$ stoichiometry.

Application of hydrostatic pressure *in silico* shows that there is a pressure range where the formation of ternary silver fluorides $AgMF_4$ is favoured over binaries. The calculated range of stability is about 7–15 GPa for $AgCuF_4$, 8–15 GPa for $AgNiF_4$, and 0–22 GPa for $Ag^{I}Co^{III}F_4$, meaning that in these conditions each system has a negative enthalpy of formation with respect to substrates. The nickel system appears to be interesting in terms of electronic structure because at 10 GPa it should form the separate layers polymorph with a narrow band gap of about 0.62 eV, less than half of that for $AgF_2$. Regretfully, none of the system studied would be metallic or would feature electronically doped $AgF_2$ sheets. The Co system is overdoped in that sense that Ag(II) becomes entirely reduced to Ag(I). Thus, doping to $AgF_2$ remains a daunting target for the future studies.

Importantly, our study shows that in ternary fluorides of Ag and M (M = Ni, Cu), the $Ag^{I}M^{III}F_4$ formulation is not stable with respect to $Ag^{II}M^{II}F_4$, unlike in the known ternary oxides of these metals, $AgMO_2$. Thus, Cu(II) and Ni(II) are expected to resist oxidizing power of Ag(II) both at ambient and elevated pressures while in the fluoride environment. Compounds with a formula $Ag^{II}M^{II}F_4$ might hold strong antiferromagnetic interactions due to the presence of strong spin-polarizer Ag(II) and second magnetic cation of 3d series. Scrutiny of the strength of magnetic interactions in these systems, especially a detailed description of superexchange coupling between Ag(II) and M(II) spins, will be performed in a forthcoming study.

## Conflicts of interest

There are no conflicts to declare.

## Acknowledgements

This work was supported by Polish National Science Center (NCN) within Beethoven project (2016/23/G/ST5/04320). The research was carried out using supercomputers of Interdisciplinary Centre for Mathematical and Computational Modelling (ICM), University of Warsaw, under grant number GA76-19. Dr Derzsi acknowledges the ERDF, R&I Operational Program (ITMS2014+: 313011W085), Scientific Grant Agency of the Slovak Republic grant (VG 1/0223/19) and the Slovak Research and Development Agency grant (APVV-18-0168).

## Notes and references

1 J. Gawraczyński, D. Kurzydłowski, R. A. Ewings, S. Bandaru, W. Gadomski, Z. Mazej, G. Ruani, I. Bergenti, T. Jaroń, A. Ozarowski, S. Hill, P. J. Leszczyński, K. Tokár, M. Derzsi, P. Barone, K. Wohlfeld, J. Lorenzana and W. Grochala, *Proc. Natl. Acad. Sci. U. S. A.*, 2019, **116**, 1495–1500.
2 D. Kurzydłowski, M. Derzsi, P. Barone, A. Grzelak, V. Struzhkin, J. Lorenzana and W. Grochala, *Chem. Commun.*, 2018, **54**, 10252–10255.
3 W. Grochala and R. Hoffmann, *Angew. Chem., Int. Ed.*, 2001, **40**, 2742–2781.
4 W. Grochala and Z. Mazej, *Philos. Trans. R. Soc., A*, 2015, **373**, 20140179.
5 A. Grzelak, M. Derzsi and W. Grochala, *Inorg. Chem.*, 2021, **60**, 1561–1570.
6 S. Bandaru, M. Derzsi, A. Grzelak, J. Lorenzana and W. Grochala, *Phys. Rev. Mater.*, 2021, **5**, 064801.
7 R. Hoppe and G. Siebert, *Z. Anorg. Allg. Chem.*, 1970, **376**, 261–267.
8 G. Stebert and R. Hoppe, *Naturwissenschaften*, 1971, **58**, 95–96.
9 C. Shen, L. C. Chacón, N. Rosov, S. H. Elder, J. C. Allman and N. Bartlett, *C. R. Acad. Sci., Ser. IIc: Chim.*, 1999, **2**, 557–563.
10 N. Bartlett, G. Lucier, C. Shen, W. J. Casteel, L. Chacon, J. Munzenberg and B. Žemva, *J. Fluorine Chem.*, 1995, **71**, 163–164.
11 B. Žemva, K. Lutar, A. Jesih, W. J. Casteel, A. P. Wilkinson, D. E. Cox, R. B. Von Dreele, H. Borrmann and N. Bartlett, *J. Am. Chem. Soc.*, 1991, **113**, 4192–4198.
12 J. Grannec, A. Yacoubi, A. Tressaud and L. Rabardel, *Solid State Commun.*, 1988, **68**, 363–367.
13 J. Curda, W. Klein, H. Liu and M. Jansen, *J. Alloys Compd.*, 2002, **338**, 99–103.
14 Y. J. Shin, J. P. Doumerc, P. Dordor, C. Delmas, M. Pouchard and P. Hagenmuller, *J. Solid State Chem.*, 1993, **107**, 303–313.
15 T. Sörgel and M. Jansen, *Z. Anorg. Allg. Chem.*, 2005, **631**, 2970–2972.
16 W. Stählin and H.-R. Oswald, *Z. Anorg. Allg. Chem.*, 1969, **367**, 206–208.
17 H. Muguerra, C. Colin, M. Anne, M.-H. Julien and P. Strobel, *J. Solid State Chem.*, 2008, **181**, 2883–2888.
18 M. AI-Mamouri, P. P. Edwards, C. Greaves and M. Slaski, *Nature*, 1994, **369**, 382–384.
19 W. Grochala, R. Hoffmann, J. Feng and N. W. Ashcroft, *Angew. Chem., Int. Ed.*, 2007, **46**, 3620–3642.
20 Y. Liu-Xiang, Z. Jing-Geng, Y. Yong, L. Feng-Ying, Y. Ri-Cheng and J. Chang-Qing, *Chin. Phys. Lett.*, 2006, **23**, 426–427.
21 A. Grzelak, J. Gawraczyński, T. Jaroń, D. Kurzydłowski, A. Budzianowski, Z. Mazej, P. J. Leszczyński,

V. B. Prakapenka, M. Derzsi, V. V. Struzhkin and W. Grochala, *Inorg. Chem.*, 2017, **56**, 14651–14661.
22 G. Kresse and J. Hafner, *J. Phys.: Condens. Matter*, 1994, **6**, 8245–8257.
23 G. Kresse and J. Furthmüller, *Phys. Rev. B: Condens. Matter Mater. Phys.*, 1996, **54**, 11169–11186.
24 G. Kresse and D. Joubert, *Phys. Rev. B: Condens. Matter Mater. Phys.*, 1999, **59**, 1758–1775.
25 J. P. Perdew, A. Ruzsinszky, G. I. Csonka, O. A. Vydrov, G. E. Scuseria, L. A. Constantin, X. Zhou and K. Burke, *Phys. Rev. Lett.*, 2008, **100**, 136406.
26 A. I. Liechtenstein, V. I. Anisimov and J. Zaanen, *Phys. Rev. B: Condens. Matter Mater. Phys.*, 1995, **52**, R5467–R5470.
27 S. L. Dudarev, G. A. Botton, S. Y. Savrasov, C. J. Humphreys and A. P. Sutton, *Phys. Rev. B: Condens. Matter Mater. Phys.*, 1998, **57**, 1505–1509.
28 J. A. Barreda-Argüeso, S. López-Moreno, M. N. Sanz-Ortiz, F. Aguado, R. Valiente, J. González, F. Rodríguez, A. H. Romero, A. Muñoz, L. Nataf and F. Baudelet, *Phys. Rev. B: Condens. Matter Mater. Phys.*, 2013, **88**, 214108.
29 M. Cococcioni and S. de Gironcoli, *Phys. Rev. B: Condens. Matter Mater. Phys.*, 2005, **71**, 035105.
30 C. Miller and A. S. Botana, *Phys. Rev. B*, 2020, **101**, 195116.
31 D. Kurzydłowski, *Crystals*, 2018, **8**, 140.
32 L. C. Ming, M. H. Manghnani, T. Matsui and J. C. Jamieson, *Phys. Earth Planet. Inter.*, 1980, **23**, 276–285.
33 D. C. Lonie and E. Zurek, *Comput. Phys. Commun.*, 2011, **182**, 372–387.
34 *XtalOpt – Publications*, http://xtalopt.github.io/pub.html, accessed October 2, 2020.
35 A. V. Krukau, O. A. Vydrov, A. F. Izmaylov and G. E. Scuseria, *J. Chem. Phys.*, 2006, **125**, 224106.
36 K. Momma and F. Izumi, *J. Appl. Crystallogr.*, 2011, **44**, 1272–1276.
37 U. Herath, P. Tavadze, X. He, E. Bousquet, S. Singh, F. Muñoz and A. H. Romero, *Comput. Phys. Commun.*, 2020, **251**, 107080.
38 W. Setyawan and S. Curtarolo, *Comput. Mater. Sci.*, 2010, **49**, 299–312.
39 P. Fischer, D. Schwarzenbach and H. M. Rietveld, *J. Phys. Chem. Solids*, 1971, **32**, 543–550.
40 W. Massa and D. Babel, *Chem. Rev.*, 1988, **88**, 275–296.
41 B. Žemva, K. Lutar, L. Chacon, M. Fele-Beuermann, J. Allman, C. Shen and N. Bartlett, *J. Am. Chem. Soc.*, 1995, **117**, 10025–10034.
42 W. Grochala, *Phys. Status Solidi B*, 2006, **243**, R81–R83.
43 In fact, during standard geometry optimization process a smooth transition between both HP1 and LP polymorphs occurred (*i.e.* optimization of HP1 polymorph at 0 GPa gave LP structure and also optimization of LP polymorph at 10 GPa led to HP1 structure).
44 A. J. Bard, R. Parsons, J. Jordan and International Union of Pure and Applied Chemistry, *Standard potentials in aqueous solution*, M. Dekker, New York, 1985.
45 J. Lapasset, P. Sciau, J. Moret and N. Gros, *Acta Crystallogr., Sect. B: Struct. Sci.*, 1986, **42**, 258–262.
46 J. Zaanen, G. A. Sawatzky and J. W. Allen, *Phys. Rev. Lett.*, 1985, **55**, 418–421.